

# Analysis of the Surface Morphology and Chemical Composition of Zr-Nb<sub>3</sub>Sn Alloys with Different Zr Concentrations

FERMILAB-PUB-24-0427-TD

**Micah Sue**

*Community College Internship (CCI) Program, Fermilab*

## **Abstract**

In the field of superconducting science, Nb has been the material of choice for Radio Frequency (RF) Cavities for years. However, in recent years Nb<sub>3</sub>Sn has shown to be a promising alternative to Nb. Its combination of a significantly high superconducting transition temperature and a much higher value of upper critical magnetic field ( $H_{c2}$ ), has been the reason the alloy has been so widely studied. This project aims to develop materials to further improve the high magnetic field performance of Nb<sub>3</sub>Sn by improving its upper critical magnetic field and critical current density ( $J_c$ ). One way to improve the  $J_c$  and the  $H_{c2}$  is to create more grain boundaries in the Nb<sub>3</sub>Sn alloy allowing them to trap more magnetic flux lines in the materials. To do this the grains must be made smaller which will naturally cause the formation of more grain boundaries. A common way to create smaller grains is by doping an impurity in the alloy. In this study, Nb<sub>3</sub>Sn was doped with Zr to form Zr-Nb<sub>3</sub>Sn alloys. This project investigates the surface properties and chemical composition of Zr-Nb<sub>3</sub>Sn alloys with varying zirconium concentrations (~0.5% and ~24% Zr). Using Scanning Electron Microscopy (SEM), Energy Dispersive Spectroscopy (EDS), and X-ray Photoemission Spectroscopy (XPS), allowed for the characterization of the differences in surface morphology and elemental composition between samples. SEM images were quantified using ImageJ giving insight into grain distribution. The results indicate that increased Zr concentration creates smaller grains in the Zr-Nb<sub>3</sub>Sn alloy. Furthermore, the ~24% Zr grew nanoscale particles on the surface that are possible oxides. XPS data revealed that as Zr concentration increased, the total Nb oxides (NbO<sub>x</sub>) thickness decreased. Conversely, as Zr concentration increased, the surface Sn oxides (SnO<sub>x</sub>) also increased slightly. Quantification via ImageJ of SEM data showed that the ~0.5% Zr sample had a grain size of ~5300 nm<sup>2</sup>. These results show that Zr inclusion leads to smaller grain formations, which is promising in the world of superconducting RF cavities for high magnetic field applications.

## **I. Introduction**

Nb is the most popular contemporary superconducting alloy used for the development of Radio Frequency (RF) Cavities. Nb<sub>3</sub>Sn is a promising replacement in RF cavities for the current metal of choice Nb. Nb<sub>3</sub>Sn has a much higher transition temperature ( $T_c$ ) and retains its superconductivity at higher magnetic fields[1]. This has caused much research has been done to improve this alloy's performance at higher and higher magnetic fields. Some specific applications of RF cavities, including axion dark matter research, require them to be operated in the presence of multi-Tesla magnetic field [2]. To improve the already high magnetic field tolerance of the alloy different approaches must be used. One such approach to improving this alloy's critical magnetic field is to decrease the grain size of Nb<sub>3</sub>Sn. Smaller grains increase the number of grain boundaries that act as flux pinning centers for the current, improving a superconductor's ability to function at higher magnetic fields. One way to do this is by adding a doping agent. In this project, Nb<sub>3</sub>Sn was doped with Zr to make Zr-Nb<sub>3</sub>Sn. The hypothesis is that increasing the concentration of Zr could make the grains of Zr-Nb<sub>3</sub>Sn smaller. To test this, two samples of Zr-Nb<sub>3</sub>Sn were examined. One sample Zr-Nb<sub>3</sub>Sn with a concentration of a Zr ~ 0.5% and another with a concentration of ~ 24% Zr. The scope of the project is as follows: studying the morphology of the two samples of Zr-Nb<sub>3</sub>Sn and their respective grain size distribution as well as conducting elemental and oxide surface analysis.

## **II. Technical Approach and Methods**

### **A. Scanning Electron Microscopy (SEM)**

The grains of Zr-Nb<sub>3</sub>Sn are not observable with the human eye or with assistance from traditional optics such as a confocal microscope. Therefore to image the two samples, Scanning Electron Microscopy (SEM) was used to observe the Zr-Nb<sub>3</sub>Sn grains. SEM uses an electron gun that shoots a beam of electrons that pass through a series of lenses and strike the sample and are scattered back at a detector forming an image. This process gives the experimenter an increased range of resolution allowing insight into even nanoscale features. Both samples were imaged with SEM with the same settings with a maximum of 100,000x magnification.

### **B. Energy Dispersive Spectroscopy (EDS)**

After being imaged with SEM for Zr-Nb<sub>3</sub>Sn, Zr ~ 24% an Energy Dispersive Spectroscopy (EDS) was used to analyze the composition of some nanoscale surface particles. EDS works by using a secondary detector that analyzes backscattered electrons inside the SEM machine. Using EDS, we tested different areas or points of interest on the samples.

### **C. X-ray Photoemission Spectroscopy (XPS)**

Following SEM and EDS, X-ray photoemission spectroscopy (XPS) was used to identify which elements are present on the surface of the two samples. XPS uses X-rays to excite electrons in a sample. When the X-rays hit the sample, electrons are emitted from the surface of the sample. These photoelectrons are emitted and analyzed by detectors. The detected energy is then analyzed, and this information is used to determine the elemental composition. The XPS data was calibrated

with the Carbon 1s peak and analyzed using a combination of Gaussian-Lorentzian and Lorentzian Asymmetric line shapes.

#### D. ImageJ Analysis

The final phase of the material analysis was using ImageJ to analyze the grain distribution of Zr-Nb<sub>3</sub>Sn using an image taken by the SEM. By using a variety of parameters a grain distribution was created which gave insight into the overall grain formation in the sample.

### III. Results and Discussion

#### A. Surface Morphology

The SEM imaging showed observable grains at 400 nm resolution with clear and observable grains for the ~ 0.5% sample as seen in Fig 1a. Conversely, no grains could be observed on the ~ 24% sample. However, the ~ 24% did have some nanoscale particles formed on the surface Fig 1b. Further investigation into these particles is discussed in the EDS results. To observe the grains in the ~24% Zr sample better resolution or the usage of a different instrument such as Transmission Electron Microscopy should be utilized.

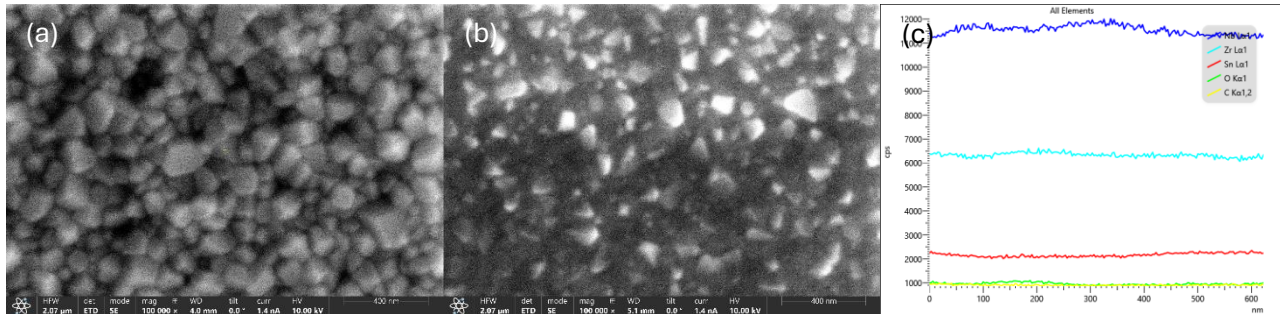


**Figure 1, SEM Images and EDS data. (a) SEM image of ~0.5% Zr sample at 100,000x magnification shows grain boundaries of sample. (b) SEM image of ~24% Zr sample at 100,000x magnification shows no grain boundaries but nanoscale particles. (c) EDS Signal Comparison ~24% Zr shows a slightly elevated oxygen count**

#### B. Elemental Composition

The EDS scan was done using a line scan. A line scan collects data from a line of interest as seen in Appendix Fig 1. This technique allows for investigation into the elemental composition of surface features. The results showed that these surface features and the background are composed of O, C, Nb, Sn, and Zr which was expected as seen in Appendix Fig 2 An analysis of the signal in Figure 1c. showed an elevated count of oxygen ranging ( in the position range of 100-250 nm) implying that these nanoscale particles are possible oxides. However, further testing including the testing of additional spots and longer scan times is required to support this claim.

#### C. XPS

The XPS data provided insight into the relative thickness of both the Nb and Sn oxides in two different samples. However, to measure the relative thickness the data had to be calibrated first.

This was done in the CASA XPS software using the Carbon 1s peak to shift the binding energy at 285.0eV, as seen in the appendix Fig 3. Nb and Sn metal to oxide signal was calculated based on the peak fits. Additionally, the relative atomic % was tabulated for NbO<sub>x</sub> in appendix table. The metal signal-to-oxide ratio shows that NbO<sub>x</sub> decreases in thickness as Zr concentration increases (Table 2) while SnO<sub>x</sub> increases in thickness as Zr concentration increases (Table 3).

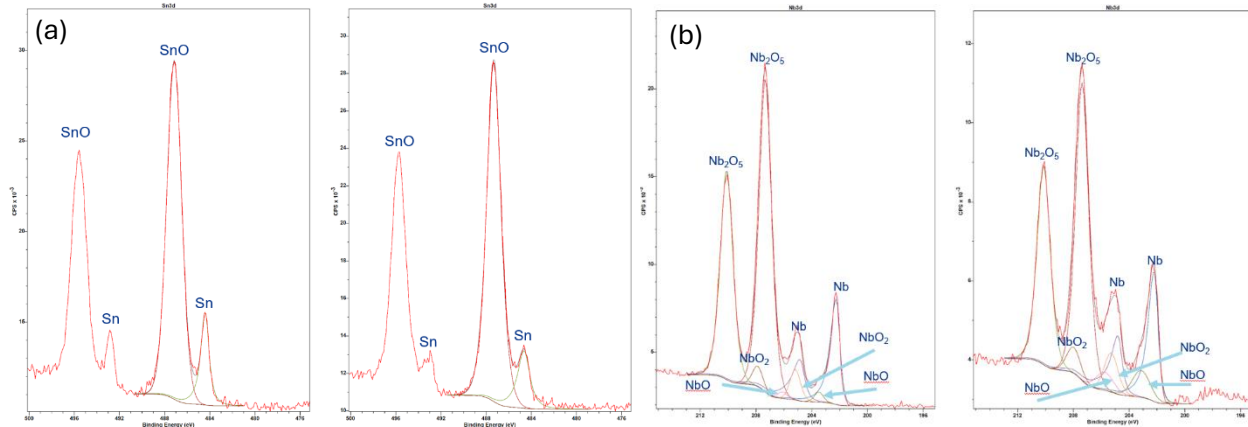


**Figure 2**, XPS Metal Peak fits. (a) Comparison of the Sn peaks in ~0.5% and ~24% samples show Sn Peak fit SnO and Sn peaks. (b) Comparison of the Nb peaks in ~0.5% and ~24% samples show Nb Peak fit shows Nb, NbO, Nb<sub>2</sub>O<sub>5</sub>, NbO<sub>2</sub> peaks in the fit.

Sample	Zr ~ 0.5%	Zr ~ 24%
Nb <sub>2</sub> O <sub>5</sub> 3d 5/2	71.52	61.11
Nb 3d 5/2	21.29	23.57
NbO 3d 5/2	1.56	7.19
NbO <sub>2</sub> 3d 5/2	5.63	8.14

**Table 1**, comparison of relative atomic % between Zr ~ 0.5% and Zr ~ 24%

Sample	Zr ~ 0.5%	Zr ~ 24%
Nb/NbO <sub>x</sub>	0.270487	0.308346

**Table 2**, comparison of relative atomic % between Zr ~ 0.5% and Zr ~ 24%

Sample	Zr ~ 0.5%	Zr ~ 24%
Sn/SnO <sub>x</sub>	0.191697	0.175748

**Table 3**, comparison of relative atomic % between Zr ~ 0.5% and Zr ~ 24%

## D. Grain Size Distribution

To obtain the grain boundary mapping seen in Figure 3b. the following method was followed and developed during this research. First, the scale was set to a known distance, in this case, 400 nm. Second, a bandpass filter with an upper limit of 25 pixels and a lower limit of 3 pixels was applied to flatten the image. Next, the image type was changed to 8-bit. This allowed for a threshold to be applied. This step has no specific parameters, so it is up to the analyst to determine the proper threshold. Finally, the watershed algorithm was applied which split the grains. This created the following grain maps as seen in Figure 3b. After tabulating results from the analyze particles function in Table 4. the software found 474 grains in the image as well as an average grain size of 5300 nm<sup>2</sup>.

**Table 4**, Data from Grain Analysis

	Zr ~ 0.5%
Number of Grains	474
Average Area per Grain (nm <sup>2</sup> )	5298.6
Number of Grains per Area (μm <sup>2</sup> )	164.87

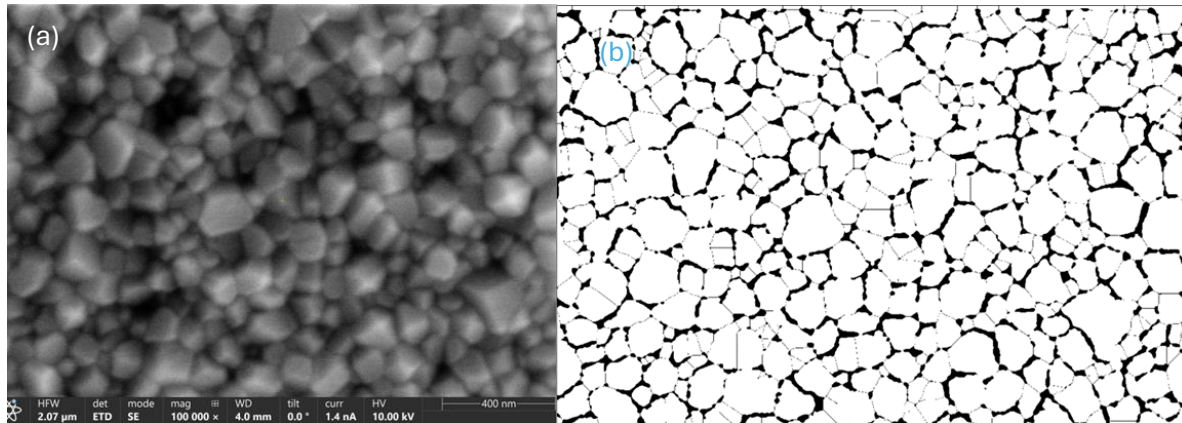


**Figure 3,** Comparison Between SEM image of ~0.5% Zr sample and its grain boundary map. (a) SEM image of ~0.5% Zr sample at 100,000x. (b) Grain boundary map of SEM image created using ImageJ software allows the grains to be counted by software

#### IV. Future Work

Future research will focus on a third sample of ~ 2.5% Zr concentration and imaging the grains of ~ 24% sample. After following the previous methods a comparison between all three samples correlating grain size to concentration of Zr will be done. The comparative data set for Nb<sub>3</sub>Sn with all three Zr concentrations will give us a correlation to how Zr inclusion affects the microstructural properties of Nb<sub>3</sub>Sn.

#### V. Impact on Laboratory or National Missions

This project aligns with the Department of Energy (DOE) and Fermi National Accelerator Laboratory (Fermilab) missions by contributing to the advancement of materials used in high-energy physics applications. The takeaway from this research is the better understanding and a route to improve the materials for superconducting RF cavities, which can be used in axion dark matter research.

#### VI. Conclusions

The results of this research show that grain size decreases with increasing Zr concentration. The formation of nanoscale particles on the ~ 24% Zr sample shows evidence of being oxides. Third XPS data showed that the NbO<sub>x</sub> decreases in thickness as the concentration of Zr increases, conversely, the SnO<sub>x</sub> slightly increases in thickness with increasing Zr concentration. Finally, ImageJ analysis shows the average grain area for the sample with ~ 0.5% Zr to be around 5300 nm<sup>2</sup>.

#### VII. References

1. A. Godeke, A Review of the Properties of Nb<sub>3</sub>Sn and Their Variation with A15 Composition, Morphology, and Strain State, *Supercond. Sci. Technol.* **19** R68
2. S. Posen *et. al*, High-Quality-Factor Superconducting Cavities in Tesla-Scale Magnetic Fields for Dark-Matter Searches, *Phys. Rev. Applied*, **20**, 034004 (2023).
3. Schneider, C., Rasband, W. & Eliceiri, K. NIH Image to ImageJ: 25 years of image analysis. *Nat Methods* **9**, 671–675 (2012)

## VIII. Acknowledgements

This manuscript has been authored by Fermi Research Alliance, LLC under Contract No. DE-AC02-07CH11359 with the U.S. Department of Energy, Office of Science, Office of High Energy Physics.

This work was supported in part by the U.S. Department of Energy, Office of Science, Office of Workforce Development for Teachers and Scientists (WDTS) under the Community College Internship (CCI)

## IX. Appendix

### A. Participants

- Micah Sue, CCI, University California Berkeley, project lead
- Malvika Tripathi, Fermilab, Supervisor
- Adam Clairmont, Fermilab, Staff Engineer 1, XPS Training
- Anna Misiewicz, Fermilab, Associate Engineer, SEM Training

### B. Scientific Facilities

Applied Physics and Superconducting Technology Directorate

Helios 5CX

SPECS XPS

### C. Figures

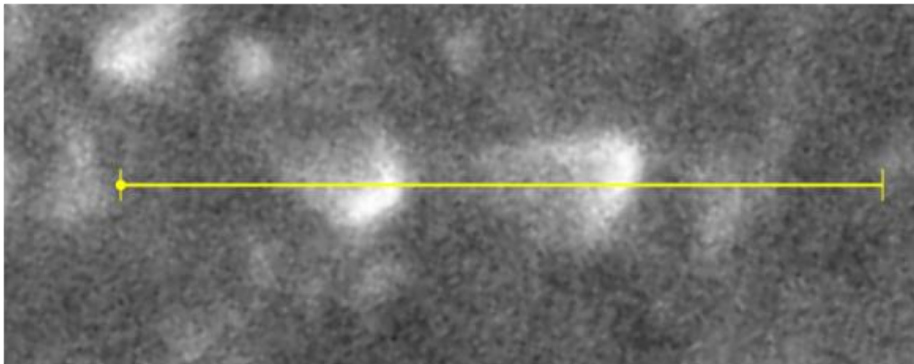


*Figure 1, EDS line scan across to nanoscale particles from the ~24% Zr sample*

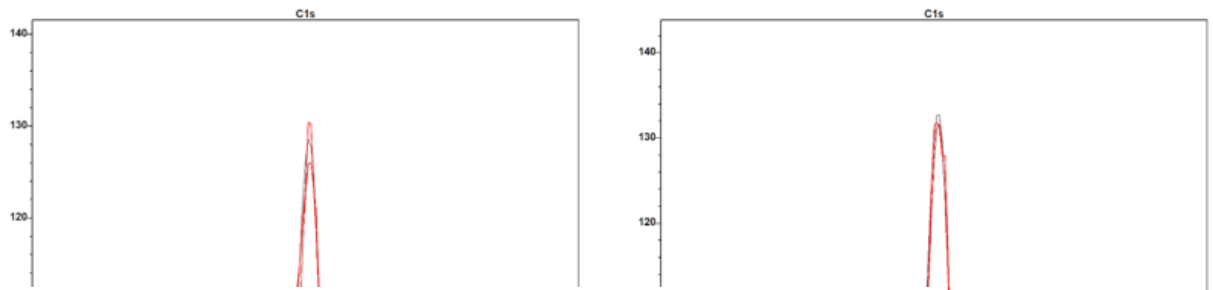


**Figure 2.** EDS elemental spectra from line-scan shows the expected elements occur in nanoscale particles

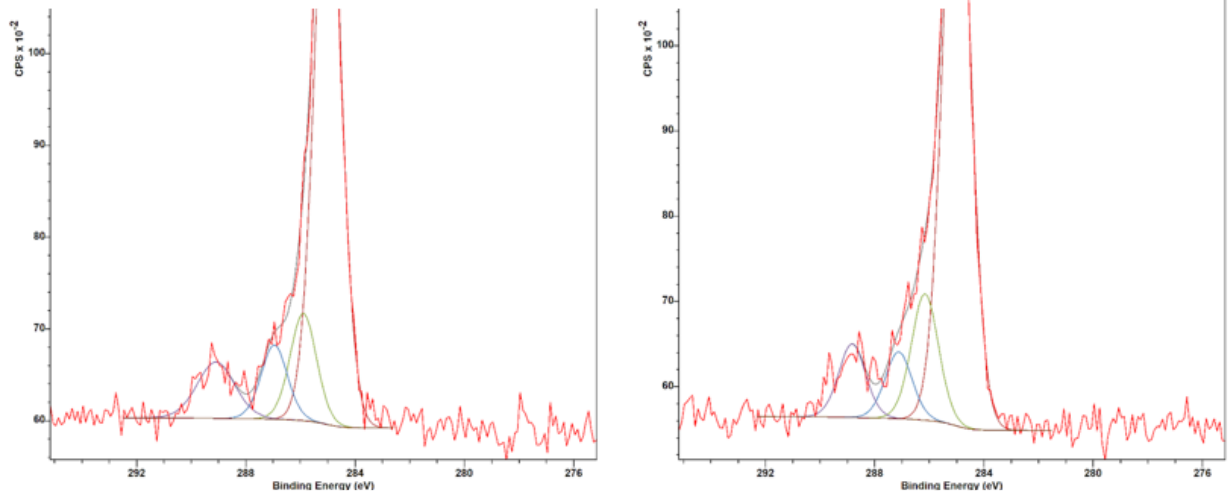


**Figure 3.** The Carbons 1s peaks used for the binding energy calibration for both samples.

